R. & M. No. 3519

ROYAL AIRCRAFT ESTABLISHMENT
BEDFORD.

MINISTRY OF TECHNOLOGY

AERONAUTICAL RESEARCH COUNCIL

REPORTS AND MEMORANDA

The Heating of Air by 'Dark' Discharge

By J. E. Hesselgreaves, B.Sc.(Eng.), T. R. F. Nonweiler, B.Sc., Ph.D., and T. R. Foord, B.Sc., Ph.D.

LONDON: HER MAJESTY'S STATIONERY OFFICE
1967
PRICE 13*s.* 0*d.* NET

The Heating of Air by 'Dark' Discharge

By J. E. Hesselgreaves, B.Sc.(Eng.), T. R. F. Nonweiler, B.Sc., Ph.D., and T. R. Foord, B.Sc., Ph.D.

Reports and Memoranda No. 3519*
May, 1966

Summary.

A theoretical and experimental investigation is made of the heating of air by means of a 'dark' or 'Townsend' discharge, the intended application being the heating of the working fluid of a hypersonic intermittent wind tunnel. Results are presented of experiments at atmospheric pressure designed to determine the efficiency of energy conversion and to test the validity of the theoretical assumptions. The theory is used to predict the performance of a small 'pilot model' heater working at 15 atmospheres pressure.

LIST OF CONTENTS

1. Introduction
2. Theory
   2.1. Assumptions
      2.2.1. Current/voltage relationship for 'axial field' geometry
      2.2.2. Pressure rise obtainable with 'axial field' geometry
      2.2.3. Current/voltage relationship for 'radial field' geometry
      2.2.4. Energy transfer
      2.2.5. Comparison of electrode geometries
      2.3.1. 'Radial field' heater at constant radius
      2.3.2. Variable-radius heater
3. Experiments
   3.1. Apparatus
   3.2. 'Axial field' experiments
      3.2.1. Current/voltage characteristics
      3.2.2. Pressure rise
      3.2.3. Energy transfer

*Replaces A.R.C. 28 046.

3.3. 'Mixed field' experiments

3.3.1. Current/voltage characteristics

3.3.2. Pressure rise

3.3.3. Energy transfer

3.3.4. Series operation

3.4. 'Radial field' experiments

3.4.1. Current/voltage characteristics

3.4.2. Energy transfer

4. Conclusions

Acknowledgments

List of Symbols

References

Illustrations—Figs. 1 to 15

---

1. *Introduction.*

It is the purpose of this Report to investigate the use of electrostatic acceleration as a source of energy for heating a moving gas stream, the application in mind being the heating of the working fluid of hypersonic intermittent wind tunnels. Basically the principle is that molecular ions are introduced into a neutral gas and are accelerated through the gas in an electric field, which is produced by a suitable arrangement of electrodes. The ions, in travelling through the gas, communicate energy and momentum to it by collision; its total enthalpy is thus increased, and if the electrode arrangement is such as to provide field lines parallel to the direction of gas flow, total pressure is also increased.

Many different types of ion sources are possible, but the simplest and the one investigated in this paper, is the corona discharge. In this the ions are formed in a very small region of plasma caused by the local breakdown of the gas in the high field region near sharply curved surfaces of electrodes. Thus the field used to accelerate the ions and cause the energy transfer also serves to provide the source of ions; herein lies the simplicity of the method.

The use of an arc as a means of heating a moving gas stream is well known, and the primary distinctions to be drawn here are that we are suggesting the use of a 'dark' discharge within a gas, instead of an arc, and the generation of energy by the mechanical work done on a charged fluid rather than by heat conduction from a hot plasma. Thus it is to be expected that the heating will be more uniform than with the arc. The element of momentum transfer also is absent in the arc heated tunnel, but it is present in the electromagnetic cross field accelerator which, apart from using a different source of force, like the arc heater produces its power at low voltage and high current, whereas the electrostatic acceleration principle involves essentially low currents and high voltages.

The most similar application of the concept is that of the electrostatic power. This utilises the 'electric wind' of electrostatically accelerated ions to produce an increased total pressure within the working fluid, but its ability to increase the total enthalpy of the gas has not seemed before to be of any practical significance. The 'electric wind' has been known from the time of Newton and before, and Chattock appears to have been the first to present an analysis of the phenomenon[1]. Within the last few years it has been the subject of considerable research by Stuetzer[2], Robinson[3] and others, from whom the

conclusion emerges that for atmospheric air the mechanical efficiency as a blower is only about 1 per cent, although for insulating liquids it is much higher. Work has tended as a result to concentrate on the device as a pump for dielectric liquids. The principle has also been used in its 'reverse' form in the field of electrogasdynamic power generation[4], in which ions liberated at a needle emitter are forced by a moving gas against an electric field; the gas then loses energy to the ions, which is communicated to the electrodes providing the field.

With reference to the present work, in Section 2 of this Report a theoretical analysis is made, using simplifying assumptions, to express the current passed between the electrodes in terms of the applied direct voltage. The insulating containing duct is assumed to be cylindrical, and two basic electrode geometries are considered. These give field lines parallel, and perpendicular to, the cylinder axis, and are referred to as the 'axial field' and 'radial field' geometries respectively. The effect of space charge on the electric field is taken account of by the use of Poisson's equation in its appropriate forms for the solutions. The theory is developed, allowing for the limiting effect of the spark breakdown condition, with a view to providing a heater of acceptable dimensions for a hypersonic intermittent wind tunnel.

The experimental work has had two primary objectives: to check the validity of the theoretical current/voltage relationships for the two electrode geometries, and to provide an indication of the efficiency of energy transfer from the electrode to the gas. The experiments have been conducted using air at atmospheric pressure.

2. *Theory.*

2.1. *Assumptions.*

The principal assumptions made in the theory are that:

(a) The velocity due to bulk gas motion is small compared with the ion drift velocity.

(b) The ion mobility is dependent only on gas density.

(c) Direct voltage is used throughout.

(d) The effects of electrical and thermal conductivity are ignored (implying that there is no ionisation in the body of the gas), and the effect of viscosity is ignored.

2.2.1. *Current/voltage relationship for 'axial field' geometry.*

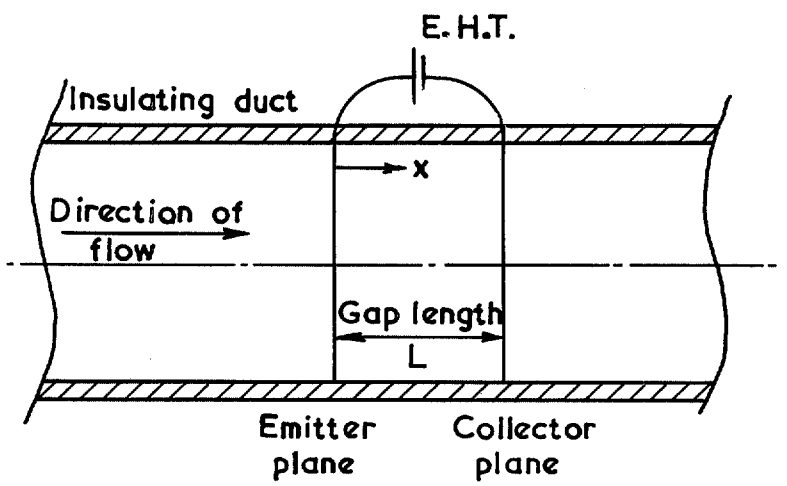

For this analysis and in the following four sections we make the additional assumptions that emission is uniform over the emitter plane, field lines are everywhere parallel to the axis, and that the duct walls have no effect on the space charge. Further, we treat the flow as incompressible so that by (b) above the ion mobility is constant.

Poisson's equation in its one-dimensional form is

$$\frac{dE_x}{dx} = \frac{\alpha\rho Q_0}{\varepsilon}. \tag{1}$$

The continuity of current is expressed by the equation

$$\frac{J}{Q_0} = \alpha v_x \rho A = \text{constant} \tag{2}$$

and the velocity of the ions v_x is related to the field strength E_x by

$$v_x = KE_x. \tag{3}$$

Eliminating the product $\alpha\rho Q_0$ from Poisson's equation we have

$$E_x \frac{dE_x}{dx} = \frac{J}{\varepsilon AK}. \tag{4}$$

This may be integrated for constant AK:

$$E_x^2 = \frac{2J}{\varepsilon AK}(x+x_0) \tag{5}$$

where x_0 is a constant of integration.
Putting $P^2 = 2J/\varepsilon AK$, equation (5) becomes

$$E_x = P(x+x_0)^{\frac{1}{2}} \tag{6}$$

which since $E_x = -dV/dx$, may be integrated to give the potential distribution. Putting V zero at the collector ($x = L$) we have

$$V = -\frac{2P}{3}(x+x_0)^{3/2} + \frac{2P}{3}(L+x_0)^{3/2}. \tag{7}$$

Let the applied potential be V_2 at the emitter. Then we have

$$V_2 = \frac{2P}{3}\left[(L+x_0)^{3/2} - x_0^{3/2}\right].$$

Substituting for P, the current for a given potential V_2 is

$$J = \eta . \frac{9\varepsilon AKV_2^2}{8L^3} \tag{8}$$

where

$$\eta = \left[\left(1+\frac{x_0}{L}\right)^{3/2} - \left(\frac{x_0}{L}\right)^{3/2}\right]^{-2}.$$

Now since x_0 is always positive, η is always less than unity; thus maximum current for a given applied voltage is obtained when x_0 is very small compared with L. From equation (6), x_0 is determined by the field at the emitter:

$$E_x^{*2} = \frac{2Jx_0}{\varepsilon AK}. \tag{9}$$

E_x^* may be regarded as a constant, being the field required at the emitter to produce corona. Then eliminating J between (8) and (9) we find

$$\eta x_0/L = (2E_x^* L/3V_2)^2 .$$

Thus x_0/L is small if V_2 is large compared with $E_x^* L$.

2.2.2. *Pressure rise obtainable with 'axial field' electrode geometry.*

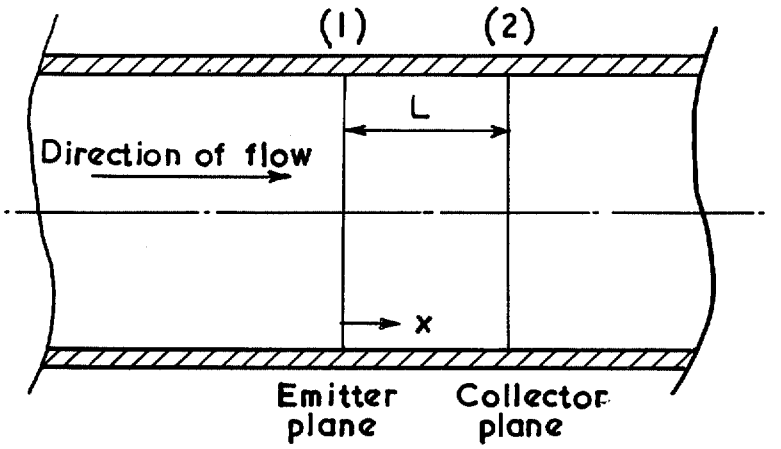

We wish to find the pressure rise between the emitter and collector planes in terms of the electrical quantities. The emitter and collector planes are referred to as stations (1) and (2) respectively, and an 'intake' pressure of n atmospheres is assumed.

The momentum equation is

$$q\,dq + \frac{1}{\rho}dp = \frac{\alpha v_x Q_0}{K}dx = \frac{Jdx}{\rho AK}. \tag{10}$$

Dividing through by q, we have

$$dq + \frac{A}{\dot{m}}dp = \frac{J}{\dot{m}K}dx. \tag{11}$$

Since A, $\dot{m}$, J, are constant over the gap length L, we may integrate over the gap length, provided that we treat K as constant;

$$\frac{A}{\dot{m}}(p_2 - p_1) + (q_2 - q_1) = \frac{JL}{\dot{m}K}$$

whence

$$\frac{p_2-p_1}{p_1} = \frac{JL}{AKp_1} - \gamma M_1^2 \quad \frac{q_2-q_1}{q_1} \tag{13}$$

where M_1 is the inlet Mach number.

Now provided that $M_1 \ll 1$, the last term may be neglected, giving

$$\frac{p_2-p_1}{p_1} = \frac{JL}{AKp_1}. \tag{14}$$

Substituting for the current in terms of the applied voltage from equation (8), equation (14) becomes

$$\frac{p_2-p_1}{p_1} = \frac{9\varepsilon E^2\eta}{8p_1} \tag{15}$$

where E represents the mean field defined by $E = V_2/L$. Now the maximum value of E, which is that of spark breakdown, is dominantly proportional to gas density. If we neglect the effect of temperature we have that E is proportional to pressure, and

$$\frac{p_2-p_1}{p_1} \quad \frac{9\varepsilon}{8p_1} . n^2 E_B^2 \tag{16}$$

where suffix B denotes breakdown at atmospheric pressure. Now the present experiments have shown that $(V_2/L)_B$ for a typical 'axial field' electrode system is 10 kv/cm. Substitution of this value into equation (16) gives

$$\frac{p_2-p_1}{p_1} \doteq 10^{-4} n. \tag{17}$$

Thus the maximum pressure rise is proportional to the inlet working pressure, but 10^4 atmospheres starting pressure would be needed if the pressure rise were to be doubled, for a single stage. If 100 stages are stacked in series, 100 atmospheres would yield the same result.

Let us now suppose that the pressure rise is used to induce gas flow through the duct. Assume that the pressure-loss coefficient of the collector (usually a wire mesh screen) is C_s; the losses due to the emitter are usually negligible. Suppose that the system operates with air at atmospheric pressure.

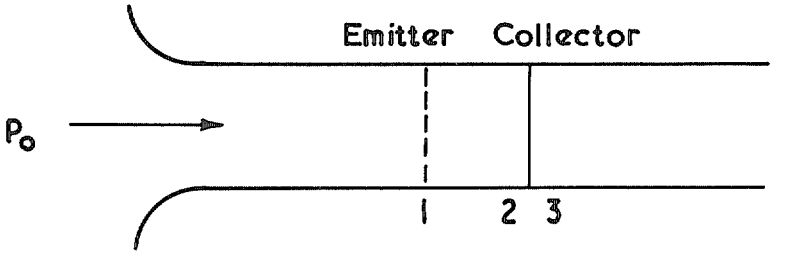

With reference to the diagram, the boundary conditions are:

$$p_3 = p_0 = p_1 + \tfrac{1}{2}\rho_1 q_1^2 \tag{18}$$

and

$$p_2 - p_3 = \tfrac{1}{2}\rho_2 q_2^2 C_s . \tag{19}$$

Since the change in density is ignored, $q_1 = q_2$, $\rho_1 = \rho_2$.

$$\text{Hence } p_2 - p_1 = \frac{1+C_s}{2}\rho_1 q_1^2 . \tag{20}$$

We now have an expression for the pressure rise in terms of the induced velocity. Using equation (14), the induced velocity is given in terms of the current:

$$q_1 = \left(\frac{2JL}{AK(1+C_s)\rho_1}\right)^{\frac{1}{2}} . \tag{21}$$

2.2.3. *Current/voltage relationship for radial field geometry.*

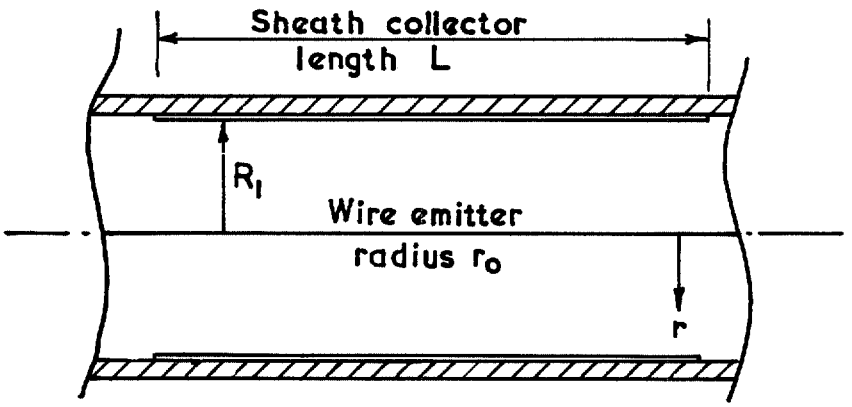

The electric field in this geometry is produced between a wire on the axis which acts also as emitter, and a concentric cylinder mounted on the inside of the insulating duct. We consider a section of length L.

Poisson's equation in the form pertaining to radial symmetry is

$$\frac{1}{r}\frac{d}{dr}(rE_r) = \frac{\alpha\rho Q_0}{\varepsilon} . \tag{22}$$

For continuity of current we have

$$\frac{J}{LQ_0} = 2\pi r\alpha v_r \rho = \text{constant} \tag{23}$$

and the mobility equation is

$$v_r = KE_r . \tag{24}$$

Eliminating $\alpha\ \rho\ Q_0$ and v_r from equations (22) to (24) we obtain for Poisson's equation

$$\frac{d}{dr}(rE_r) = \frac{J}{2\pi L\varepsilon K}\cdot\frac{1}{E_r} . \tag{25}$$

so that V_2 can never exceed $V_{\lim} = E_r^*(R_1 - r_0)$. In fact, of course, spark breakdown may occur before this limit is reached. In general, we can deduce from (27) and (29) by eliminating ϕ that

$$V_2 = \psi^{\frac{1}{2}}(R_1 - r_0)/\eta^{\frac{1}{2}}$$

$$\text{where } \eta^{-\frac{1}{2}} = \left\{ g\left(\frac{E_r^{*2}}{\psi} - 1\right)\frac{r_0^2}{R_1^2}\right] - g\left(\frac{E_r^{*2}}{\psi} - 1\right)\left(\frac{r_0}{R_1}\right)\right\} \Big/ \left(1 - \frac{r_0}{R_1}\right) \tag{32}$$

$$\text{and } g(\chi) = (1+\chi)^{\frac{1}{2}} - \chi^{\frac{1}{2}} \sinh^{-1} \chi^{\frac{1}{2}}.$$

Thus from (31) $\eta \to 1$ as $\psi/E_r^{*2} \to 1$, and $\eta \to 0$ as $\psi \to 0$. Clearly also as $r_0/R_1 \to 0$ we see that $\eta \to 1$ from below. From (32) and the definition of ψ we have

$$J = 2\pi\varepsilon LK\eta(V_2/R_1)^2 \tag{33}$$

where η therefore reaches its greatest value (of unity) in the limits $r_0 \to 0$ or $V_2 \to V_{\lim}$.

2.2.4. *Energy transfer.* If we assume that no heat is lost to the surroundings we have from the energy equation

$$H_2 - H_1 + \tfrac{1}{2}(q_2^2 - q_1^2) = -J\Delta V/\dot{m} \tag{34}$$

which becomes, provided that the Mach number is everywhere small,

$$\Delta H = -J\Delta V/\dot{m}. \tag{35}$$

We have already seen (Section 2.2.2.) that the relative change in pressure is so small as to be negligible provided that the Mach number is small. For a heater with an axial field this is a manifestation of the assumption (a) that the ion velocity is high compared with the gas bulk velocity; for a radial field heater it would be a direct consequence of the assumed absence of any external axial force. Thus the speed q and M^2 each vary as H in a heater of constant cross-sectional area, and since the rise in enthalpy is always limited, equation (35) may be justified where the intake Mach number is small compared with unity.

2.2.5. *Comparison of electrode geometries.* Let us assume that each geometry operates in the same length of duct L, the radius being R_1. The same applied voltage V_2 is also assumed. For the axial field, then, the 'optimum' current/voltage relationship is (*see* Section 2.2.1.):

$$J_x = \frac{9\varepsilon\pi R_1^2 K V_2^2}{8L^3} \tag{36}$$

and for the radial field (Section 2.2.3.):

$$J_r = \frac{2\pi\varepsilon KLV^2}{R_1^2}. \tag{37}$$

Dividing (36) by (37), we have the ratio of currents

$$\frac{J_x}{J_r} = \frac{9}{16}\left[\frac{R_1}{L}\right]^4. \tag{38}$$

We see that if $R_1/L = 2/\sqrt{3}$, the current passed in each geometry is the same. If $R_1/L < 2/\sqrt{3}$ the current passed in a given volume for the radial field is greater. Thus if we are to operate the axial field geometry economically in terms of heater volume we must have a length/diameter ratio of smaller than $\sqrt{3/4}$. To achieve multiplication of power input we must stage several of these heaters in series down the tube, working at alternate polarities. This suggests introducing a neutralisation zone at least equal to the gap length, which reduces the space utilisation by half. On the other hand, inspection of equation (37) shows that with the radial field geometry this problem does not arise; to achieve multiplication of power one merely elongates the heating section, since the current is proportional to length.

The only other factor to be brought into the comparison at this stage is that of breakdown voltage. The maximum power input for each geometry occurs at breakdown voltage (V_s) and it is thus desirable to operate as near to this voltage as possible. Now the experiments (Figs. 7 and 14) have shown that V_s/R for the radial field geometry is greater than V_s/L for the axial field system. It is thus evident that, with the 'comparative' length/radius ratio derived, either the radial field system would be operating well away from the breakdown condition at the same power input, or it could give higher powers before breakdown.

It seems, then, on theoretical grounds, that the radial field electrode geometry is preferable, and we shall now investigate the performance of this type of heater for a typical set of working conditions.

2.3.1. *Radial field heater at constant radius.*

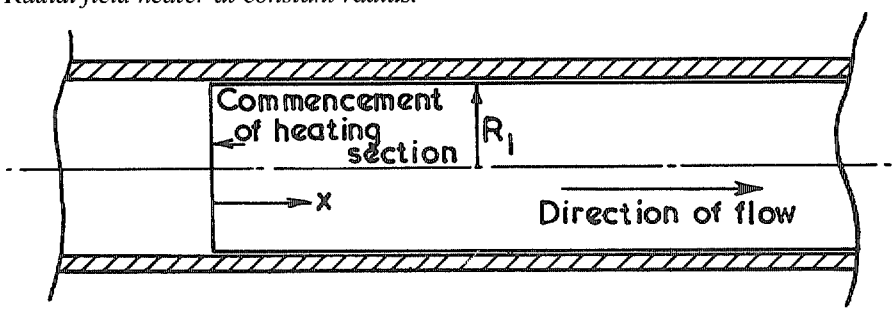

For the purposes of analysis we make the following additional assumptions to those made at the introduction to the theory:

(e) Spark breakdown strength is inversely proportional to gas density.

(f) Ion mobility is inversely proportional to gas density.

(g) Heating is uniform through any transverse section.

(h) There are no energy losses.

(i) The Mach number remains small.

Let suffix 0 denote gas properties at ambient conditions (NTP),

x denote gas properties at distance x from entry to heating section.

Consider a section at distance x from entry. Let the applied potential be V_2 and the working pressure n atmospheres (which is virtually constant if inlet Mach number is small). Then if we assume that the current per unit length at station 'x' is dependent only on the gas properties at 'x', we have, using the simplified relationship,

$$\frac{dJ_x}{dx} = 2\pi\varepsilon K_x \frac{V_2^2}{R_1^2}. \tag{39}$$

Relating the mobility to normal conditions the power gradient is

$$V_2 \frac{dJ_x}{dx} = 2\pi\varepsilon \frac{K_0}{n} \cdot \frac{T_x}{T_0} \cdot \frac{V_2^3}{R_1^2} \tag{40}$$

where T is the absolute temperature.

The temperature gradient is then given by

$$\frac{dT_x}{dJ_x} = \frac{V_2}{\dot{m} C_p}. \tag{41}$$

Thus the temperature rise in the duct up to station x is given by the differential equation

$$\frac{dT_x}{dx} = \frac{V_2}{\dot{m} C_p} \cdot \frac{2\pi\varepsilon K_0 V_2^2}{n R_1^2} \cdot T_x. \tag{42}$$

Now put

$$\Omega = \frac{2\pi\varepsilon K_0 V_2^3}{T_0 C_p R_1^2} = \text{constant}.$$

The solution to this equation is

$$\frac{T_x}{T_0} = \exp\left(\frac{\Omega x}{\dot{m} n}\right). \tag{43}$$

We now have an expression for the temperature rise in the heating section in terms of the dimensions of the section, the mass flow rate, the working pressure, and the applied voltage. Suppose we wish to attain a final temperature of 500 deg C with air at 15 atmospheres pressure, and have a power supply capable of 10 kw output at 80 kv. The voltage and temperature required, together with the assumption regarding breakdown, fix the diameter of the heater at 3·2 cm, and the power output and temperature fix the mass flow rate at 10 gm/sec, allowing for 50 per cent power losses. This would correspond to a speed of about 0·7 metre/sec at inlet, and would entail discharging through a throat of about 3 mm diameter to achieve a Mach number of 6 without liquification. Then Fig. 4 shows the temperature as a function of the length.

2.3.2. *Variable radius heater.* The above analysis is for the simplest possible type of heater, that is, one at constant voltage and of constant radius. However, it would only operate at the 'optimum' condition of near spark breakdown at the 'hot' end; upstream of this the breakdown voltage would become progressively greater than the applied voltage. In order to operate so as to gain the maximum possible utilisation of volume we must have a heater that will operate near breakdown over the whole of its length. This would entail either adjusting the applied voltage distribution along the length, or changing the radius along the length. Since the former is probably difficult and expensive to achieve in practice, we shall now investigate the performance of a 'variable radius' heater, at constant voltage.

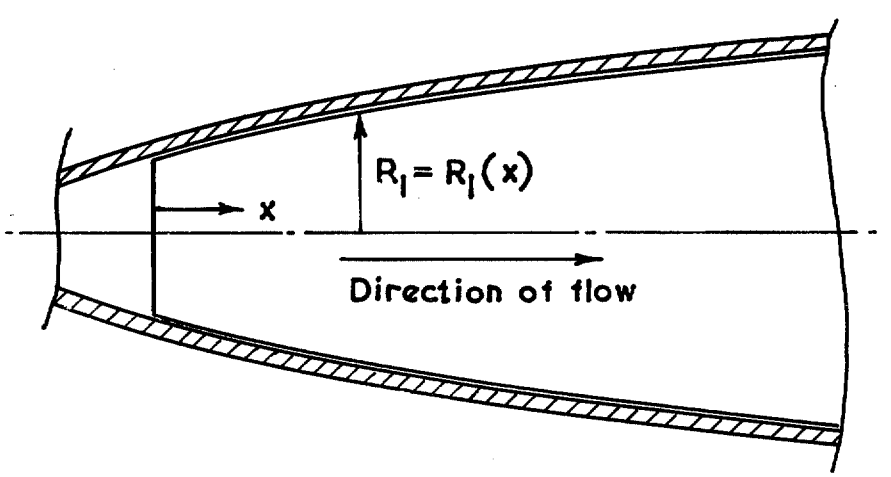

Again we start with the basic radial field relation

$$\frac{dJ_x}{dx} = 2\pi\varepsilon K_x \frac{V_2^2}{R_1^2(x)} \tag{44}$$

(which applies provided dR_1/dx is small).
The voltage V_2 is kept constant, but $(V_2/R_1(x))_{\text{Breakdown}}$ is reduced as the temperature rises, so to keep conditions near breakdown we must increase R_1 with x. From assumption (f) we have

$$\left(\frac{V_2}{R_1(x)}\right)_{\text{Breakdown}} = \left(\frac{V_2}{R_1}\right)_{\text{Breakdown}} \cdot \frac{nT_0}{T_x} \tag{45}$$

where $(V_2/R_1)_{\text{Breakdown}}$ is the voltage/gap ratio at ambient conditions at which breakdown occurs. Thus substituting (45) into (44), we have

$$\begin{aligned}\frac{dJ_x}{dx} &= 2\pi\varepsilon K_x \left(\frac{V_2}{R_1}\right)^2_{\text{Br.}} \cdot n^2 \left(\frac{T_0}{T_x}\right)^2 \\ &= 2\pi\varepsilon K_0 \left(\frac{V_2}{R_1}\right)^2_{\text{Br.}} \cdot n\left(\frac{T_0}{T_x}\right).\end{aligned} \tag{46}$$

The temperature rise in the section is given by (41)

$$\frac{dT_x}{dJ_x} = \frac{V_2}{\dot{m}C_p}$$

which becomes

$$\frac{dT_x}{dx} = \frac{T_0^2}{XT_x} \tag{47}$$

where

$$\frac{1}{X} = \frac{2\pi\varepsilon K_0}{T_0\dot{m}C_p}\left(\frac{V_2}{R_1}\right)^2_{\text{Br.}} \cdot nV_2 . \tag{48}$$

Integrating (47) with respect to x, we have

$$\frac{T_x^2}{T_0^2} = 1 + \frac{2x}{X} \tag{49}$$

whence

$$T_x = \left(2T_0^2\frac{x}{X} + T_0^2\right)^{\frac{1}{2}}. \tag{50}$$

This function is also shown plotted on Fig. 1, for the same conditions as before.

The shape of the duct required is obtained from equations (45) and (50), and is

$$R_1(x) = \frac{V_2}{(V_2/R_1)_{\text{Br.}}} \cdot \left(\frac{2x}{X}+1\right)^{\frac{1}{2}}. \tag{51}$$

This is shown plotted on Fig. 2.

3. *Experiments.*

3.1. *Apparatus.*

The experiments were conducted in a Perspex cylinder fitted with an intake, as shown schematically in Fig. 3. The whole assembly was mounted in a large wooden box to exclude draughts, the general set-up being shown in Fig. 4.

The high voltage direct current power supply consisted of a Cockcroft-Walton voltage doubling circuit (Fig. 5) capable of supplying up to 100 kilovolts at 8 milliamps, with either positive or negative polarity. Changes in ion polarity, however, were achieved by the simpler method of interchanging the HT and earth leads. Current was measured on a multirange Avometer protected by a capacitor and needle gap in parallel, and voltage by monitoring the current through a known $400M\Omega$ resistor. A spark-over trip actuated by a microphone was placed near the duct and operated on the main control relay on the primary side of the supply transformer.

The electrodes for the 'axial field' experiments were a needle or array of 17 needles acting as emitters, and a plane wire-mesh screen of 2·7 mm mesh size and 0·5 open-area ratio as collector. The single needle was mounted on the axis of the tube, while the 17-point array was designed so as to give a distribution of emission as large and as even as possible over the plane of the emitter. The distance between the points and the collector screen, defined as the gap length, was variable between about 2 and 13 cm. For the 'mixed field' geometry the emitter was a needle or spray of needles mounted on the tube axis, the collector being a brass sheath placed on the inner wall of the tube a distance downstream of the emitter. The arrangement is shown schematically in Fig. 3. Both sheath width (W) and the 'gap length' (L) were variable, from 1 to 8 cm, and 2 to 8 cm, respectively. For the 'radial field' geometry the electrodes were a brass sheath 30 cm long on the inner wall of the tube and a wire 0·33 mm dia. on the axis, supported by narrow Perspex struts.

The velocity of air through the duct was measured with a system consisting of a pitot-static tube and a Hilger – I.R.D. M.D.C. type micromanometer; to allow for the effect of low Reynolds numbers this system was calibrated as a unit. The mass flow rate of the air was calculated from the mean velocity, obtained by a pitot-static traverse (*see* Section 3.2.2.).

Measurement of the temperature rise of the air across the gap was achieved for values up to about 0·5 deg C by the 'pair-ratio' method[5] using platinum resistance thermometers. For values higher than 0·5 deg C a mercury-in-glass thermometer having 0·01 deg C divisions was used.

Since there could be no axial pressure rise with the 'radial field' electrode geometry, and hence no induced flow of air through the duct, a small centrifugal fan was used for this purpose, with the duct acting as its intake.

3.2. *'Axial Field' Experiments.*

3.2.1. *Current/voltage characteristics.* Measurements were made of the current/voltage characteristics of (a) single point-to-plane discharges, and (b) of discharges from the multi-point array to plane, at various gap lengths. The results are shown on Figs. 6 and 7 respectively, which show experimental points taken up to near spark-breakdown of the gap. Also shown on these figures is the theoretical relationship based on equation (8), which has been plotted using experimental values of ion mobility (K) and starting field strength (E_1) determined by curve fitting from the experimental results. In the case of the multi-point emitter (Fig. 7), it is seen that these values are independent of gap length, indicating that the one-dimensional theory holds very well. The values are $K = 1{\cdot}75$ cm^2/volt sec and $E_1 = 2{\cdot}14$ kv/cm.

This independence is not observed for single-point discharges (Fig. 6); the starting field E_1 drops from 2·94 to 0·46 kv/cm, with corresponding values of K rising from 0·17 to 1·42 cm^2/volt sec as gap length increases from 2·54 to 12·7 cm. While it is thought possible that the starting field could undergo the change observed, such a change in effective mobility is not physically justifiable (since air density is approximately constant). It thus appears that strong three-dimensional effects inherent in this electrode geometry render the one-dimensional theory inviable.

It is noticeable in these figures that the experimental points begin to diverge from the theoretical curves as the applied voltage approaches breakdown. This suggests that the mobility increases at the higher field strengths[6].

3.2.2. *Pressure rise.* The pressure rise between emitter and collector is related to the induced velocity by equation (20) (Section 2.2.2.); the latter quantity was measured in preference to the pressure rise directly as the measurement was easier.

Pitot-static traverses were made upstream of the emitter and downstream of the collector, and a mean velocity calculated from the upstream profiles obtained. It was found that the mean velocity was 85 per cent of the indicated centreline velocity upstream of the emitter (where the profile was very flat). The mean velocity is shown in Fig. 8, plotted against the square root of the product of current and gap length, for various gap lengths with positive ion polarity. It is seen that the velocity is a function only of this product. The theoretical relationship based on equation (21) is also shown in this figure; the screen pressure loss coefficient used was a function of velocity of the same form as that given in Ref. 7 but reduced by 30 per cent to fit the experimental points. Results obtained for single-point emitters, and for both emitters with negative ion polarity also fit the same curve.

3.2.3. *Energy transfer.* Measurements of temperature rise were made on single-stage heaters with both polarities, and are shown on Fig. 9 for the 17-point emitter with positive polarity. A set of points with negative ion polarity at 2·5 cm gap length is also shown; measurements at larger gaps were subsequently found to be subject to errors due to corona leakage from the leads outside the duct, and are therefore omitted. The measured enthalpy rise (assuming C_p = 1·00 Joule/gm deg C) is plotted against the power input divided by mass-flow rate, the latter being calculated from the measured mean velocity. The gradient of any curve drawn on this figure is thus a measure of the efficiency of energy transfer, or 'conversion efficiency', which is defined as the proportion of electrical energy converted into thermal energy of the gas. Experimental scatter prohibits the placing of an accurate figure for the efficiency, but the results indicate that there are no considerable losses. Measurements of the temperature were made difficult by 'pick-up' on the platinum resistance thermometers and by the fact that ambient temperature variations were of the same order as the temperature difference measured.

A check was made on losses from the high voltage loads outside the duct by monitoring the current in the earth and high voltage leads simultaneously, first with both electrodes in the duct, then with the collector (high voltage) removed but conditions otherwise identical. The earth lead was well shielded outside the duct. The current registered in the high voltage lead in the latter case was entirely 'leakage' current, and was equal to the difference between the currents measured in the earth and high voltage leads with both electrodes *in situ*. The leakage current increased rapidly with applied voltage, being about 30 μA at a direct voltage of 50 kv. The test showed that there was no measurable leakage of emission within the duct. Collection of charge on the wall is thought to be negligible as the stray capacitance to earth is very small (about 7 pF with sheath 30 cm long, and much less without sheath).

3.3. *'Mixed Field' Electrode Geometry.*

3.3.1. *Current/voltage characteristics.* Current/voltage characteristics were obtained for 'mixed field' electrodes with the 'gap' L (*see* Fig. 3) varying from about 2 to 8 cm, using collector sheaths of width W from 1 to 8 cm. Single and 5-point needle emitters were tested. Three typical characteristics are shown in Fig. 10. The curves show that the effect of increasing the number of emitting needles from 1 to a 'spray' of 5 is greatly to increase the maximum power input before breakdown. If gap length L is doubled the current for a given applied voltage is reduced, but the breakdown voltage is higher, and the maximum power input is little changed.

The only effect of variation of collector width W was slightly to reduce breakdown voltage if W was less than about 1 cm.

Comparison of these results with those of the 'axial field' experiments shows that a much higher power input is obtained before breakdown with this geometry. It has not proved possible, however, to provide a theoretical basis for analysis of the results in a manner similar to that of Section 2.2.1., due to the complexity of the electric field.

3.3.2. *Pressure rise.* Since aerodynamic losses with this electrode geometry are very small the pressure rise is considered equal to the dynamic head (equation (20)). Measured values of dynamic head for a single-stage heater are shown plotted against current in Fig. 11 together with the theoretical relationship based on equation (14), assuming zero pressure losses and using the measured value of mobility quoted in Section 3.1.2. It is seen that there is good agreement with theory up to about 50 microamperes, at which the rate of increase of pressure rise (with current) begins to fall off sharply. This curve is typical of many obtained with different gap lengths and different numbers of emitter points. It is assumed that the radial component of current increases as the voltage and hence total current increases; this would happen when corona started from the body of the needle in addition to the discharge from the point.

3.3.3. *Energy transfer.* Fig. 4 shows results of measurements of specific energy rise of air against specific energy input for a 'mixed field' electrode geometry of gap length $L = 3$ cm, with the 5-point emitter. Since the power input obtained was greater with this geometry, the temperatures measured were greater than with the axial field geometry and the measurements were consequently more accurate. The energy rise was close to the ideal case. A temperature traverse showed little variation of temperature across the duct.

3.3.4. *Series operation.* Three heaters were staged in series by mounting a brass strut across the diameter of the duct at the rear of each collector sheath with a needle emitter soldered at the centre of the strut, as shown in Fig. 3. The polarity of successive emitters was arranged to be alternate. In Fig. 13 the current/voltage characteristic obtained with this configuration is shown, and for comparison a characteristic of a single-stage heater of similar gap length. The results indicate that a multiplication of current for a given applied voltage is obtained, but the breakdown voltage is lower for series operation; this results in the total power input obtained before breakdown being lower than that of the single-stage system. The cause of the lower breakdown voltage is assumed to be connected with a change in the field distribution produced by the staging.

The pressure rise obtained with the staged system is shown in Fig. 11, and is compared with results for the single stage discussed above. It is seen that at low current the curves are identical; at higher currents the staged results are more in accordance with one-dimensional theory, suggesting that a greater proportion of the current is axial than with the single stage.

3.4. *Radial Field Experiments.*

Since the 'mixed field' geometry gave a greater power input for a given length of duct than the 'axial field' geometry, an electrode system giving purely radial field lines was tested.

3.4.1. *Current/voltage characteristics.* A typical set of current/voltage characteristics is shown in Fig. 14 for a 'radial field' geometry with emitter radius 0·0165 cm and collector radius 5·72 cm. It is seen that the curves for positive and negative ion polarity are similar, and it is therefore concluded that the ion mobilities are the same for the two polarities. However, spark breakdown occurs at a lower voltage with positive ion polarity. The theoretical relationship given by equation (33) is shown plotted for comparison. It is based on values of starting voltage and ion mobility (respectively 9·8 kv and 2·18 cm^2/volt sec) determined by curve fitting from the experimental results with positive ion polarity. Comparison of theory with experiment shows that the measured current increases more rapidly than the theoretical voltages above about 30 kv. This suggests that the effective ion mobility increases with increasing field strengths (c.f. Section 3.2.1.).

3.4.2. *Energy transfer.* Results of temperature measurements made with a negative emitter are shown in Fig. 15, together with the 'ideal' curve. The thermal conversion efficiency given by these tests is seen to be slightly greater than 100 per cent, indicating some small experimental error. On the basis of these tests, the total energy losses are thought to be negligible.

4. *Conclusions.*

The experiments have shown that the heating of air by a 'dark' discharge is efficient at the energy levels involved, with both axial and radial field heaters. Staging of mixed field heaters with alternate polarity was found to be possible, but only with long neutralisation zones between stages, which meant a low heater volume utilisation. A much greater power input for a given heater volume was obtained with the radial field heater.

Comparison of theoretical predictions with experimental results for the current/voltage relationship justified to a large extent the assumptions made in the theory, although there was strong evidence (*see* Sections 3.2.1. and 3.4.1.) that ion mobility tended to increase as the field strength approached the breakdown value.

For the development to a hypersonic-tunnel heater it is proposed to put into effect the ideas set out theoretically in Sections 2.3.1. and 2.3.2., involving a radial field heater. This has considerable practical advantages over a staged axial field system, particularly as regards electrode construction and insulation, in addition to the theoretical advantage mentioned in Section 2.2.5.

Since a.c. power is easier to obtain at high voltages, work will be conducted with alternating instead of direct voltage; an amendment to the theory will be necessary, but for low frequencies this is not expected to affect the functional relationship between current and applied voltage.

Acknowledgments.

The authors wish to express their gratitude to Mr. R. R. Perry of the Department of Aeronautics and Fluid Mechanics, who constructed the apparatus and gave invaluable assistance with the experiments.

LIST OF SYMBOLS

p	Static pressure of gas
ρ	Density of gas
T	Absolute temperature of gas
q	Velocity of gas
H	Specific enthalpy
$v_{x,r}$	Drift velocity of ions with respect to gas (axial and radial directions respectively)
α	Ion mass fraction
Q_0	Charge to mass ratio of singly charged ion
K	Ion mobility
E	Electric potential gradient
J	Current
V	Electric potential
ε	Gas permittivity
A	Cross-sectional area of duct
m	Mass-flow rate of gas
x	Distance along duct measured from emitter (axial electrode geometry) Distance from entry of heating section (radial electrode geometry)
r	Radial distance from axis of duct
M	Mach number
L	Length of heating section
C_p	Specific heat at constant pressure of gas
R	Gas constant
R_1	Radius of duct
x_0	Distance upstream of emitter at which axial field vanishes
r_0	Radius of emitter (radial field geometry)
P^2	$2J/\varepsilon AK$
V_2	Applied potential
E_x	Axial field strength
E_r	Radial field strength
η	(*See* equations (8) and (32))
E_x^*	Critical field for emission (axial field system)
E_r^*	Critical field for emission (radial field system)
ψ	(*See* equation (25))

ϕ	(*See* equation (26))
n	Pressure in atmospheres

Suffices o, x are used to denote gas properties at ambient conditions (NTP) and at station x respectively.

Suffices $_{1,2}$ are used to denote gas properties at emitter and collector respectively.

Dimensions where quoted are in metric units.

LIST OF REFERENCES

No.	*Author(s)*	*Title, etc.*
1	A. P. Chattock	On the velocity and mass of ions in the electric wind in air. *Phil. Mag.* Vol. 48, p. 401. 1899.
2	O. M. Stuetzer	Ion drag pressure generation. *J. appl. Phys.* Vol. 30, p. 984. 1959.
3	Myron Robinson	Movement of air in the electric wind of the corona discharge. *Trans. AIEE*, Vol. 81, p. 143. 1961.
4	A. Marks, E. Barreto and C. K. Chu	Charged aerosol energy converter. *AIAA Journal*, Vol. 2, No. 1, p. 45. 1964.
5	A. A. R. El Agib	The pair ratio method of measuring small temperature difference. J. scient. Instrum., Vol. 41, p. 592. 1964.
6	J. M. Meek and J. D. Craggs . .	*Electrical Breakdown of Gases.* Clarendon Press, Oxford, p. 31. 1953.
7	P. Jonas	The changes produced in an air stream by wire gauge. *Engineers' Digest.* Vol. 18, No. 15, p. 191. 1957.

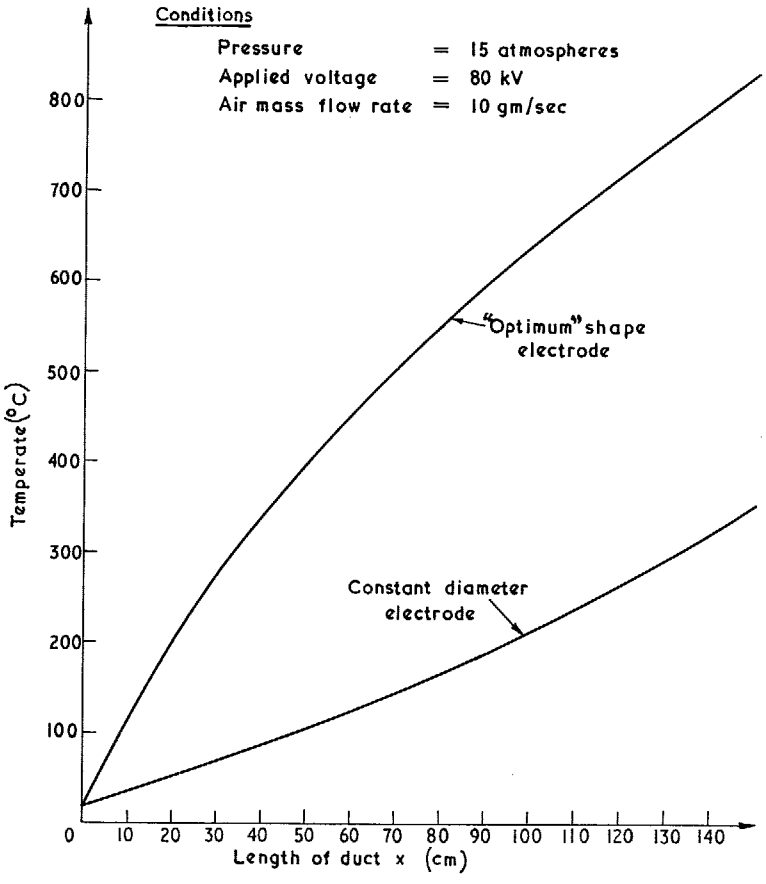

FIG. 1. Theoretical temperature attained at end of tubular heaters.

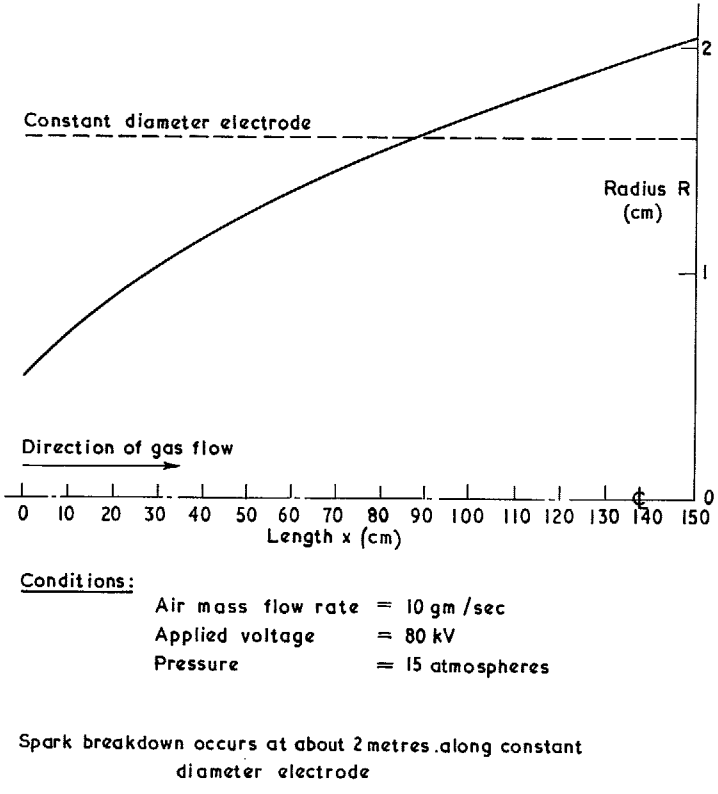

FIG. 2. Shape of 'optimum' electrode.

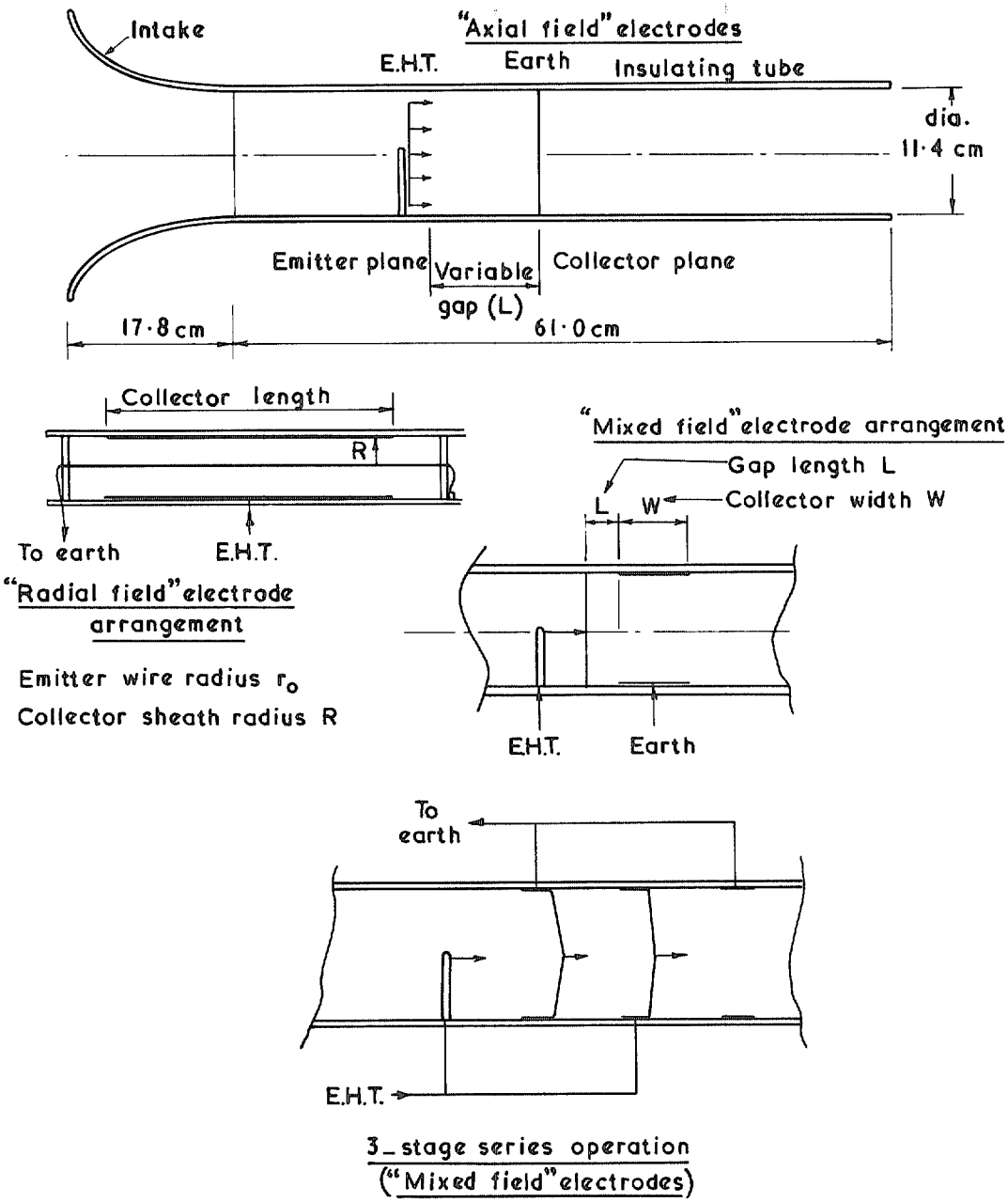

FIG. 3. Schematic diagram of apparatus.

(Not to scale).

FIG. 4. General view of apparatus.

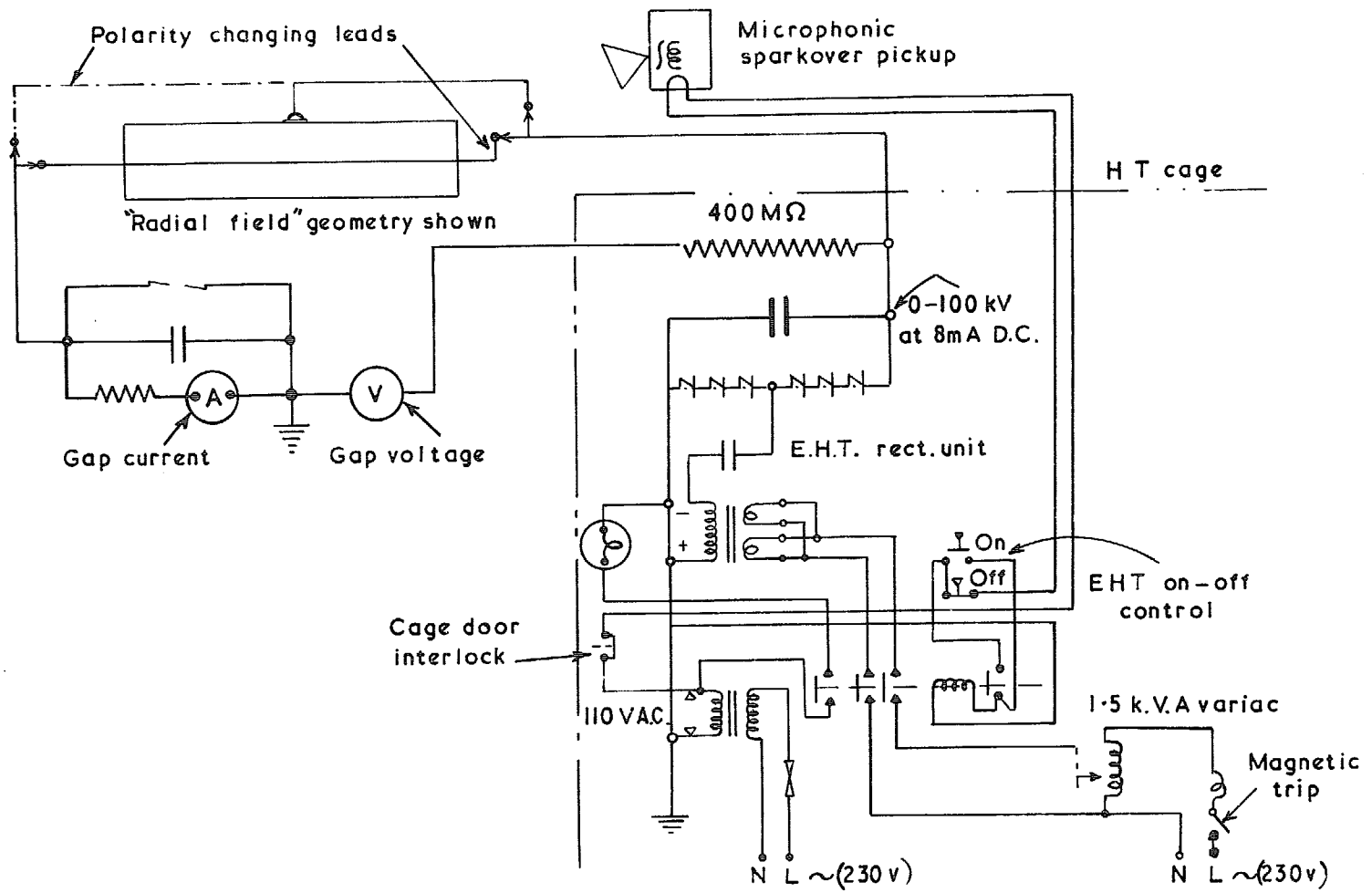

FIG. 5. Circuit diagram for d.c. operation.

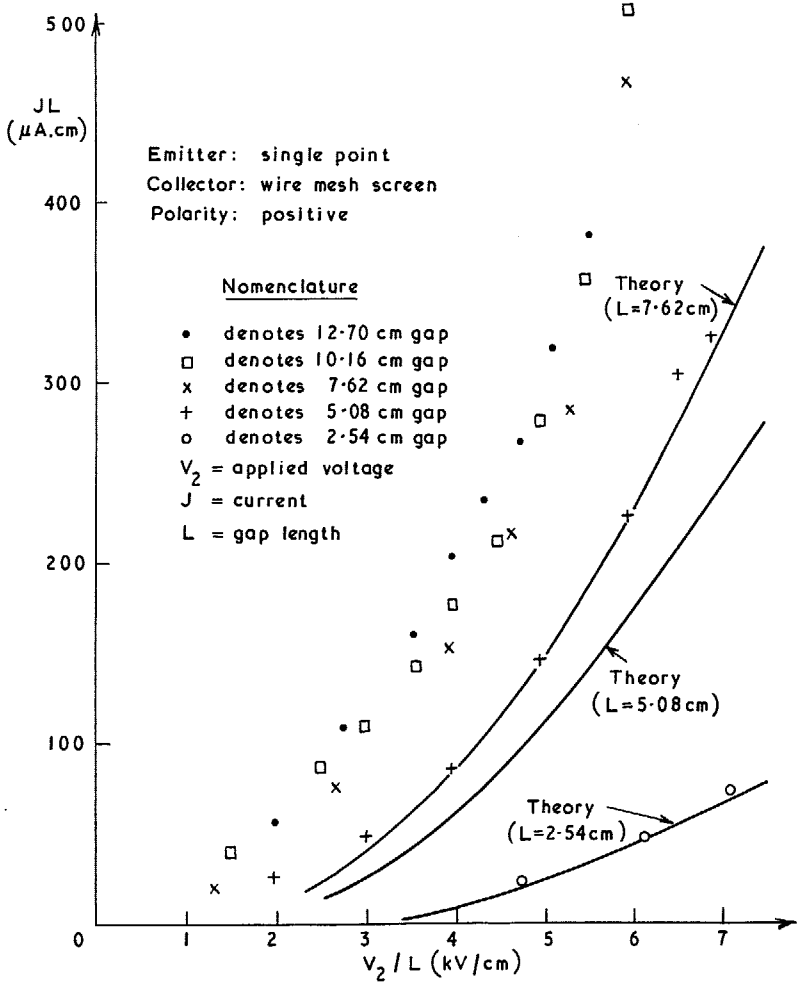

FIG. 6. Current/voltage characteristics for 'axial field' geometry.

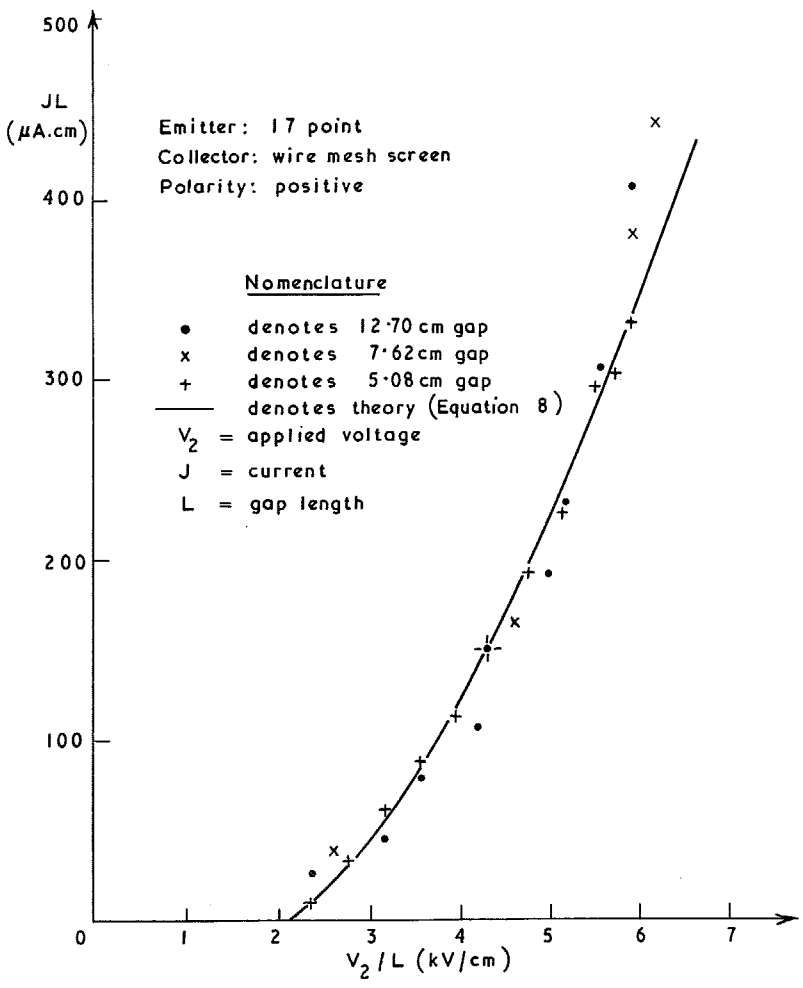

FIG. 7. Voltage/current characteristics for 'axial field' geometry.

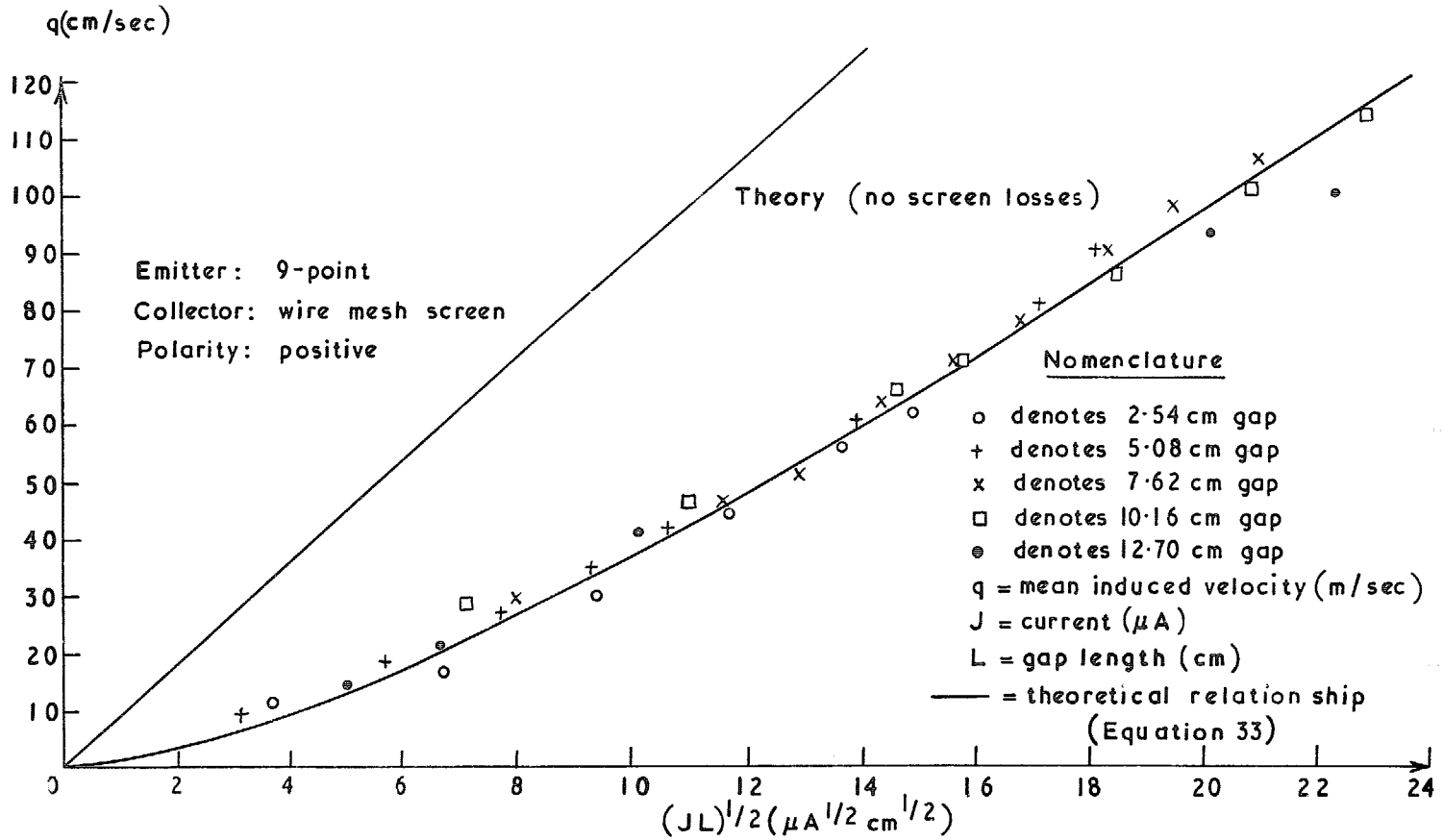

FIG. 8. Mean induced velocity for 'axial field' geometry.

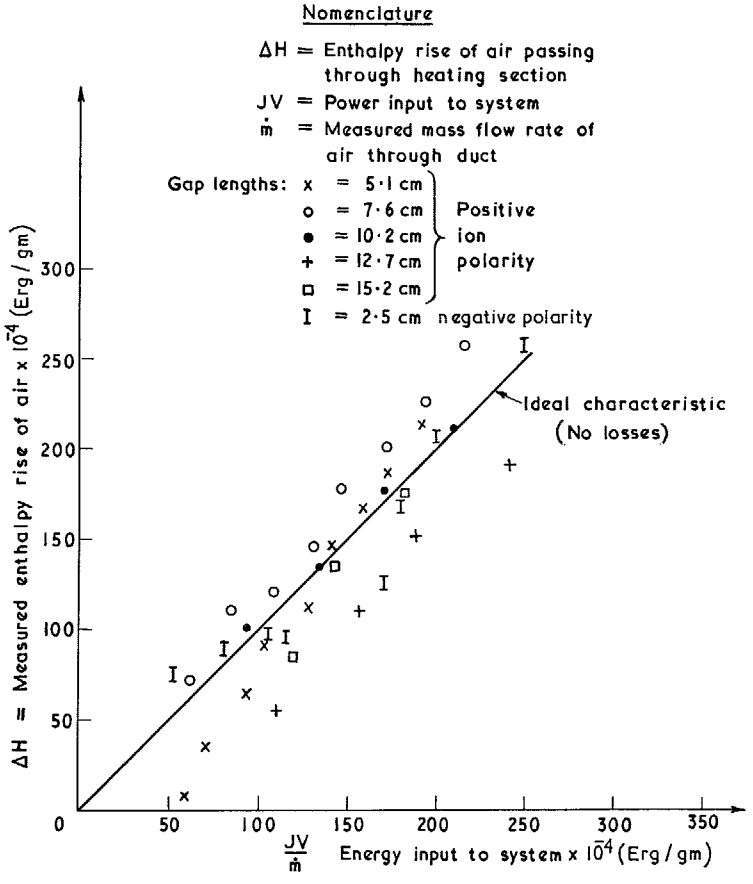

FIG. 9. Energy transfer for 'axial field' geometry.

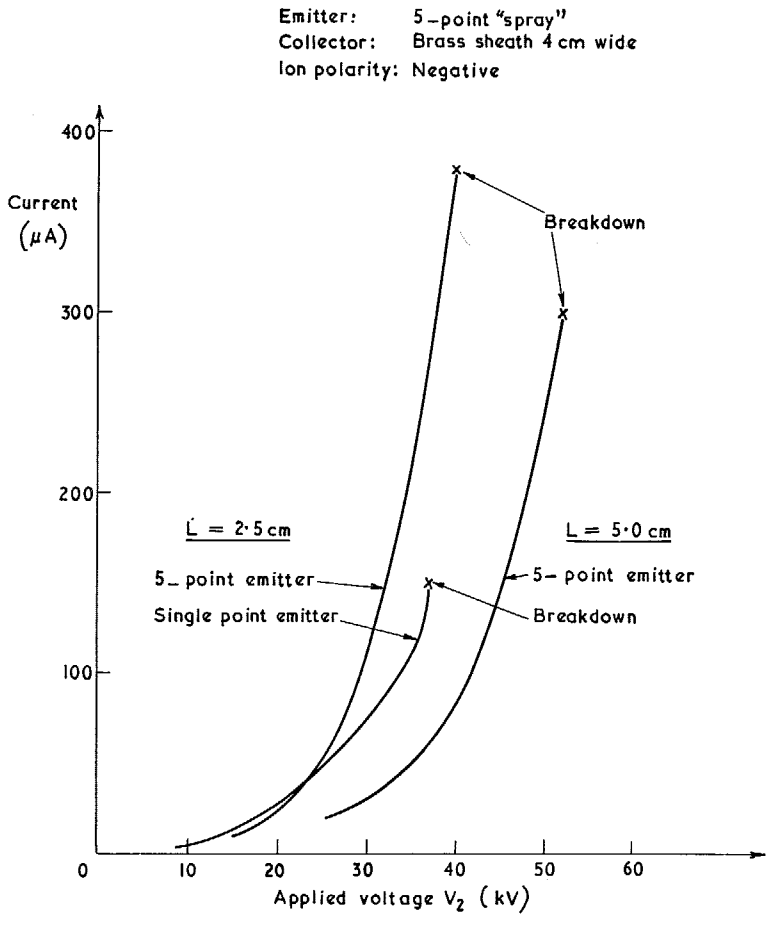

FIG. 10. Current/voltage characteristics for 'mixed field' electrodes.

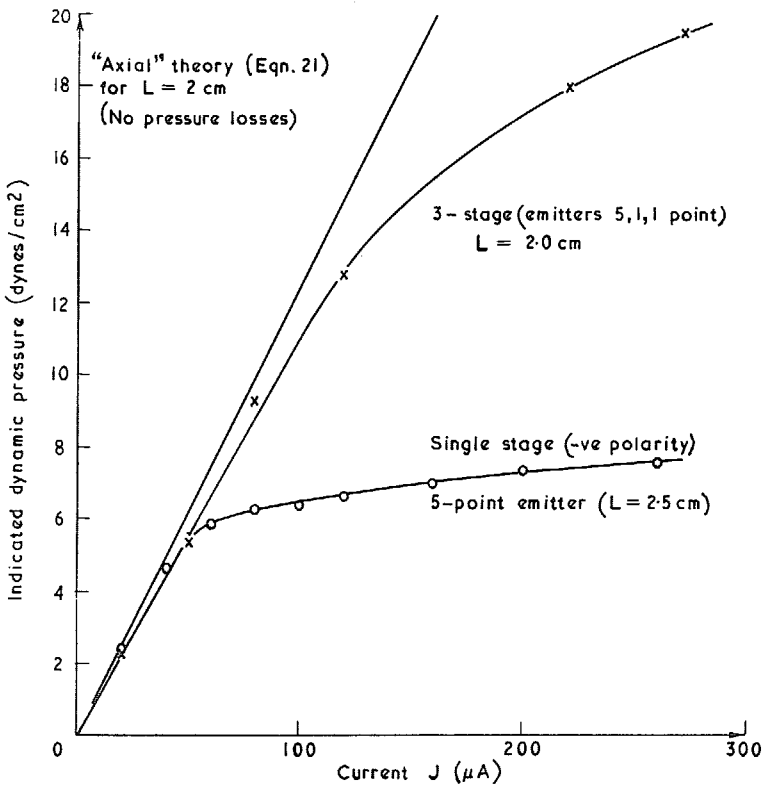

FIG. 11. Comparison of single and three stage 'mixed field' heaters. (Pressure rise versus current).

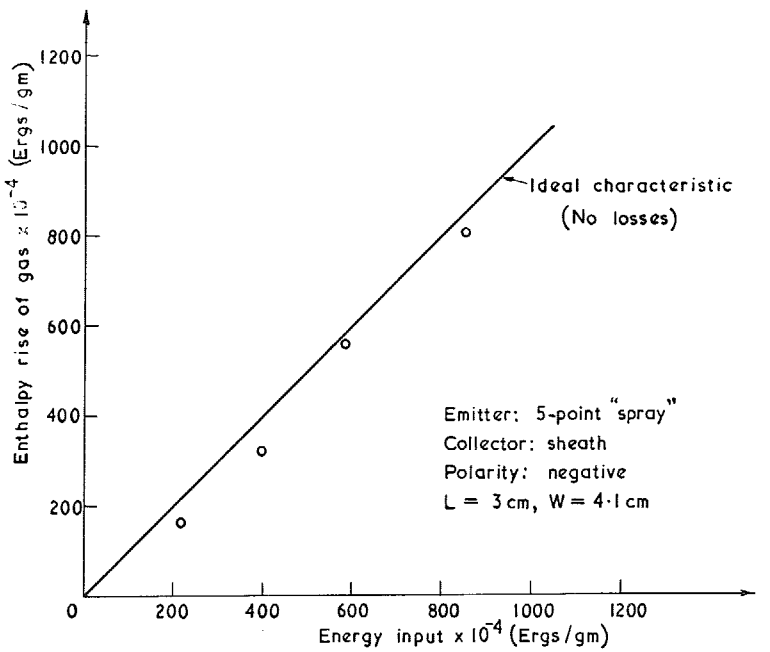

FIG. 12. Energy transfer for 'mixed' electrode system.

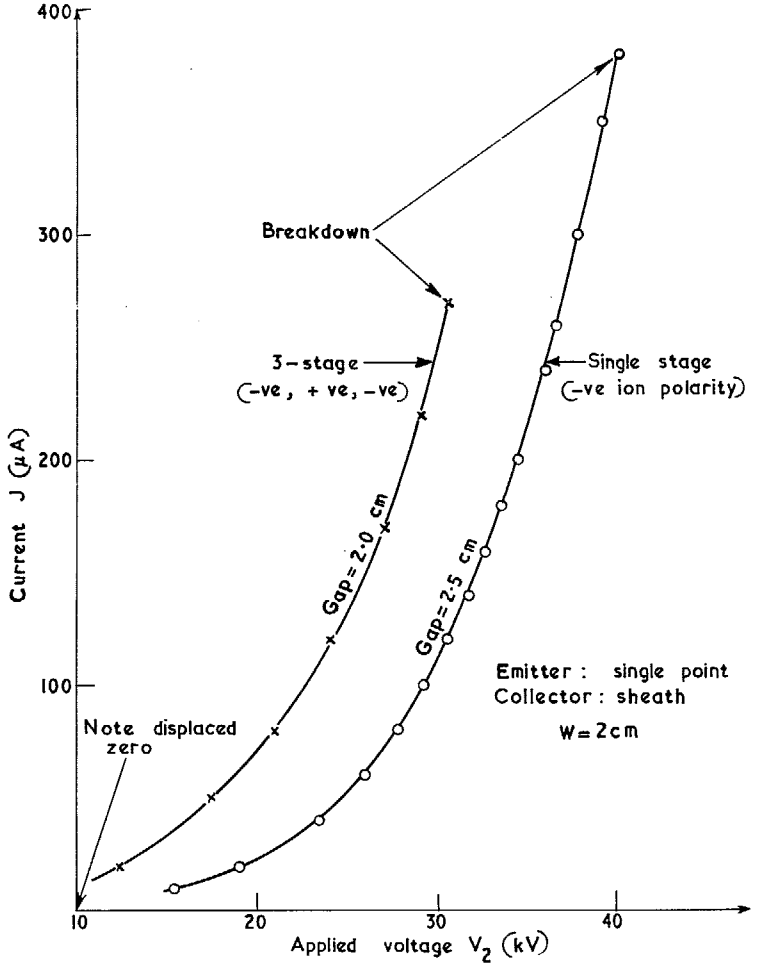

FIG. 13. Comparison of single and three stage heaters. (Current/voltage characteristics). 'Mixed field' geometry.

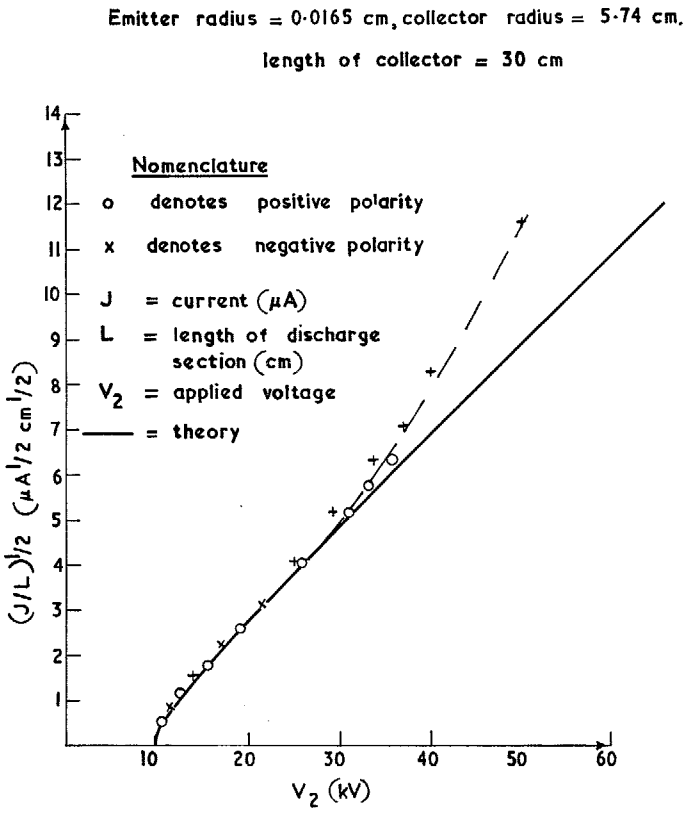

FIG. 14. Current/voltage characteristic for 'radial field' electrodes.

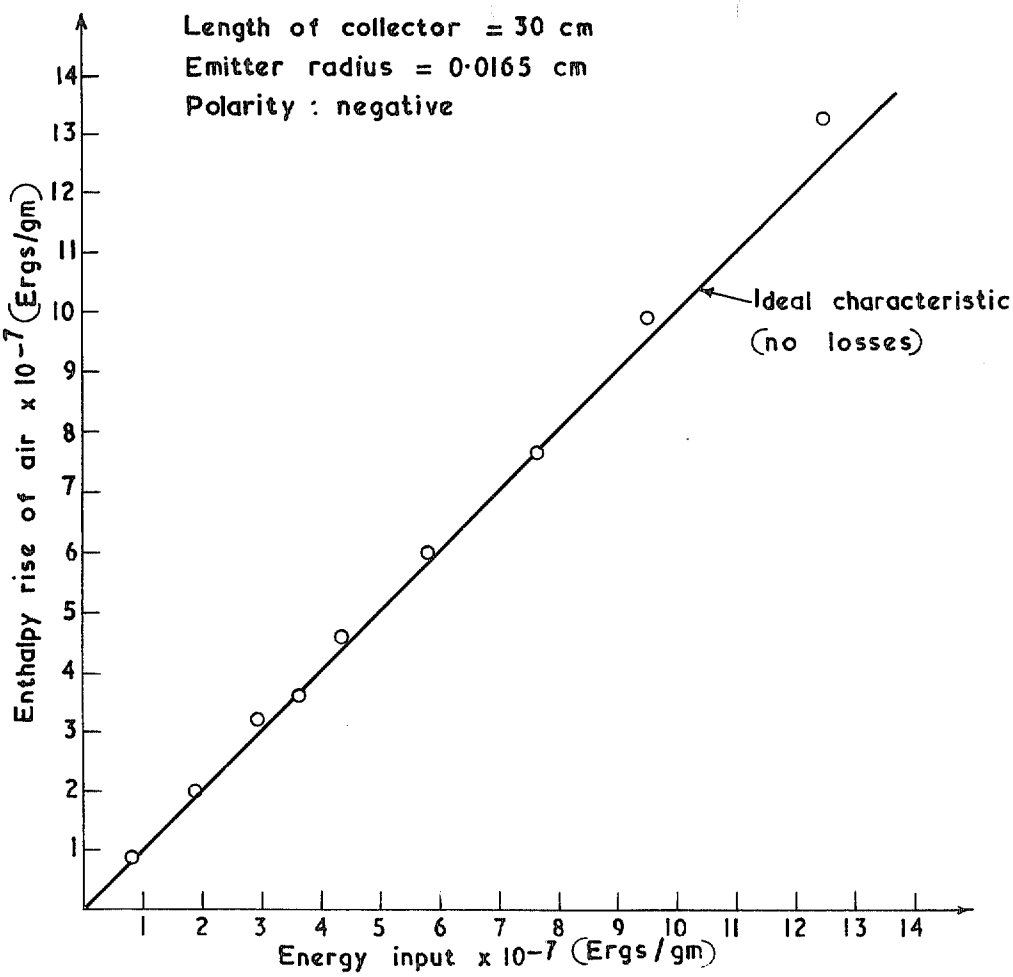

FIG. 15. Energy transfer for 'radial field' electrode system.

Printed in Wales for Her Majesty's Stationery Office by Allens Printers (Wales) Limited.

Dd.129527 K5.

© *Crown copyright* 1967

Published by
HER MAJESTY'S STATIONERY OFFICE

To be purchased from
49 High Holborn, London W.C.1
423 Oxford Street, London W.1
13A Castle Street, Edinburgh 2
109 St. Mary Street, Cardiff CF1 1JW
Brazennose Street, Manchester 2
50 Fairfax Street, Bristol 1
258–259 Broad Street, Birmingham 1
7–11 Linenhall Street, Belfast BT2 8AY
or through any bookseller

S.O. Code No. 23-35